JOURNAL OF GEOPHYSICAL RESEARCH, VOL. 97, NO. C8, PAGES 12,639–12,652, AUGUST 15, 1992

Diurnal Tides Near the Yermak Plateau

LAURIE PADMAN,[1] ALBERT J. PLUEDDEMANN,[2] ROBIN D. MUENCH,[3] AND ROBERT PINKEL[4]

Recent current measurements obtained from drifting platforms over the Yermak Plateau in the eastern Arctic Ocean confirm that the plateau is a region of greatly enhanced diurnal tidal currents. Modulation of the diurnal currents is clearly related to the plateau topography, as has been previously proposed. We show, however, that temporal variability due to spring-neap modulation must also be considered in interpreting records from drifting platforms. We review simple models of tidal current amplification in this region and find that the previous assumption of near-resonant, barotropic shelf waves propagating around the plateau's entire perimeter is inconsistent with the true topography. Instead, we propose that the diurnal variability is due to topographic shelf waves at the K_1 and O_1 tidal frequencies that are generated at points on the plateau's perimeter where the waves' group velocities are near zero. Observed cross-slope variations in ellipticity, orientation, and magnitude of tidal oscillations are consistent with the presence of topographic waves generated in this manner. The topographic enhancement of the diurnal tide near the Yermak Plateau has important consequences for the sea ice cover, hydrography, and general circulation of this region. For example, the stress divergence applied by the tidal currents at the ice base greatly exceeds the typical divergence of the surface wind stress, and tides may therefore be important to local ice deformation. The strong cross-slope tidal currents also appear to be responsible for the production of high-frequency internal wave packets, which are associated with energetic diapycnal mixing in the pycnocline. We also consider the possibility that tidal rectification is responsible for a mean current transporting Atlantic Water clockwise around the plateau.

1. INTRODUCTION

The Yermak Plateau (YP) in the eastern Arctic Ocean (Figure 1) has previously been identified as a region of enhanced tidal band variability in both the diurnal [*Hunkins*, 1986] and semidiurnal [*D'Asaro and Morison*, 1992] frequency bands. Recent studies also suggest that diapycnal mixing processes associated with the diurnal tide are important to the large-scale heat and momentum balances for this region, where the incoming Atlantic Water still retains much of its characteristic heat and salt content [*Padman and Dillon*, 1991]. *D'Asaro and Morison* [1992] found from surveys with expendable current profilers that internal wave shear variance was higher over the YP than in the deep Nansen Basin. Using the empirical model of *Gregg* [1989], they hypothesized that mixing rates were an order of magnitude higher over the YP than in the Nansen Basin owing to instabilities in the inertial and higher-frequency internal gravity waves. *Plueddemann*'s [this issue] analysis of current profiles supports this emerging view of the YP as a region of significant internal wave production, perhaps through the interaction of strong tidal currents with bottom topography.

Hunkins [1986] and *Chapman* [1989] modeled the diurnal tide in this region as a near-resonant, forced topographic wave propagating around an axisymmetric submarine plateau. Numerical studies of the global ocean tides [e.g., *Schwiderski*, 1980] do not resolve any significant diurnal tidal enhancement in this region, possibly because of coarse grid resolution relative to cross-slope topographic scales. A recent numerical model of tides in the Nordic seas and Arctic Ocean [*Gjevik and Straume*, 1989; *Gjevik*, 1990] employed a finer grid (50 km) and predicted some current amplification near the YP. The model failed, however, to generate currents as large as those reported by Hunkins. The model also predicted that maximum currents would be found over the shallow central plateau rather than over the upper slope as suggested by Hunkins' measurements. These results did not change substantially when the grid resolution was reduced to 25 km (B. Gjevik, personal communication, 1991).

Recent oceanographic programs in the region [see *Padman and Dillon*, 1991; *Muench et al.*, 1992; *Plueddemann*, this issue] have added substantially to the available regional data base. In addition, a number of satellite-tracked drifters that have crossed the YP have shown significant diurnal motion [*Hoffman*, 1990; *Prazuck*, 1991]. Given the importance of the tide to other oceanographic processes, it is now appropriate to reinvestigate the diurnal tide near the YP and to evaluate its consequences for the larger-scale hydrography and circulation of the eastern Arctic Ocean.

In this paper we review the available current and hydrographic data sources in this region (section 2) and then describe the tidal current and hydrographic variability (section 3). Models that might explain the observed energetic diurnal tides are discussed in section 4 and are compared with available data in section 5. Finally, we qualitatively discuss the role of tidal enhancement in the large-scale heat and momentum budgets of this region (section 6).

2. DATA SOURCES

Several experiments have been carried out in the vicinity of the YP in the last several years, and those relevant to the present study are listed in Table 1. The locations of these experiments are shown in Figure 1. The recent Coordinated Eastern Arctic Experiment (CEAREX) and the Arctic environmental drifting buoy (AEDB) are discussed in sections 2.1 and 2.2, respectively. Other experiments are summarized in section 2.3.

[1]College of Oceanography, Oregon State University, Corvallis.
[2]Woods Hole Oceanographic Institution, Woods Hole, Massachusetts.
[3]Science Applications International Corporation, Bellevue, Washington.
[4]Marine Physical Laboratory, Scripps Institution of Oceanography, La Jolla, California.

Copyright 1992 by the American Geophysical Union.

Paper number 92JC01097.
0148-0227/92/92JC-01097$05.00

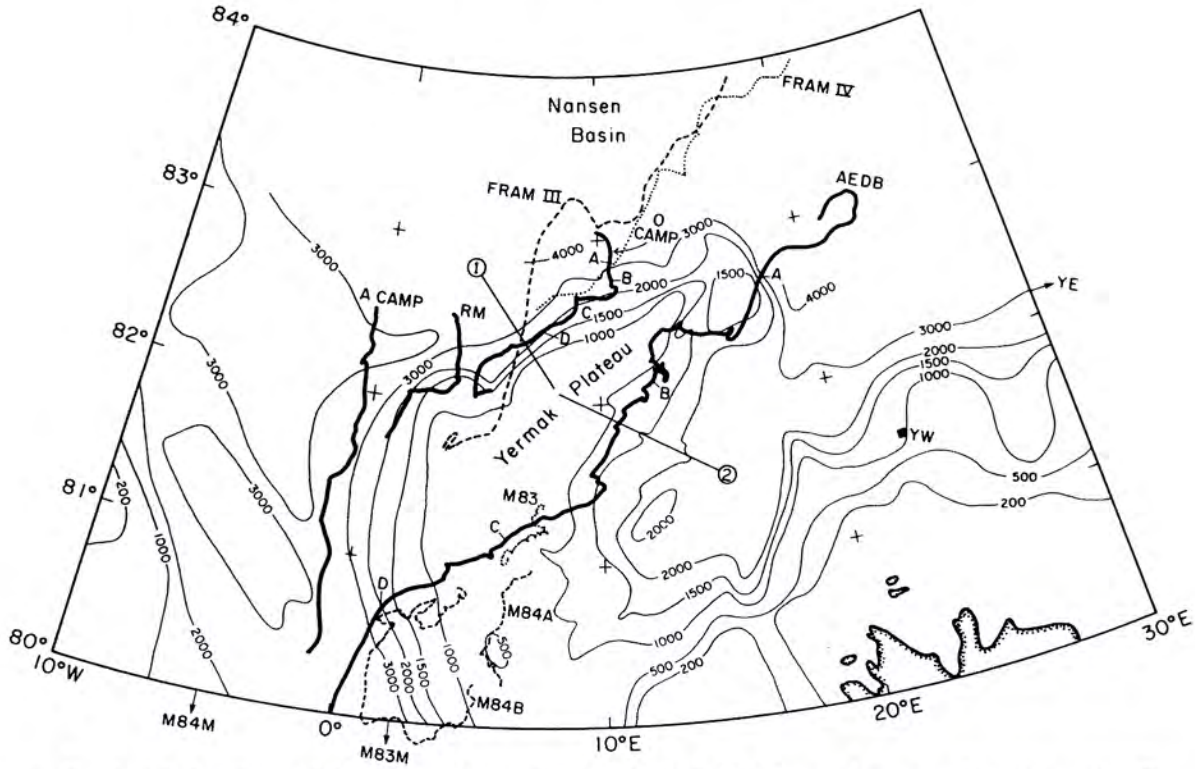

Fig. 1. The locations of field programs discussed in the text: CEAREX O camp, A camp, and remote mooring (O CAMP, A CAMP and RM respectively); the Arctic environmental drifting buoy (AEDB); MIZEX 83 ship drift (M83); MIZEX 84 ship drift (M84A and M84B); YMER west (YW) and YMER east (YE) moorings; Fram III and Fram IV ice camps; and MIZEX 83 and MIZEX 84 moorings (M83M and M84M respectively). Transects marked "1" and "2" refer to cross-slope topographies used in section 4.3. Points marked "A," "B," "C," and "D" on the O camp and AEDB tracks are discussed in the text. Water depths are in meters.

2.1. *The Coordinated Eastern Arctic Experiment*

CEAREX was a multiplatform program designed to study a wide range of oceanographic and atmospheric processes in the eastern Arctic Ocean. We will concentrate on the ice camp phase conducted in spring 1989, in which two manned ice camps and an unmanned mooring site drifted for several weeks within the study region (Figure 1). The mean drift was approximately southward with the Transpolar Drift [*Moritz and Colony*, 1987]. In each case the local ice motion was determined from approximately hourly satellite positions and then smoothed with the complex demodulation algorithm described by *McPhee* [1988]. This algorithm is intended to reduce the errors involved in each position estimate (about 100 m) by assuming that the ice responds only to the wind (low frequency), tides (diurnal and semidiurnal), and inertial currents. The principal features of these drifts and the large-scale hydrographic conditions of the region have been described by *Muench et al.* [1992].

TABLE 1. Sources of Current Meter Data Used in the Present Study

Experiment	Location	Mooring Type*	Year	Reference
YMER	Barents Sea slope	M	1980	*Aagaard* [1989]
Kvitøya	Barents Sea slope	M	1981	*Aagaard et al.* [1983]
Fram III	Nansen Basin	D	1981	*Johnson* [1983]
	NW slope of YP			*Hunkins* [1986]
Fram IV	Nansen Basin	D	1982	*Johnson* [1983]
	NW slope of YP			*Hunkins* [1986]
MIZEX 83	central Fram Strait	M	1983	*Hunkins* [1984]
MIZEX 83	central YP	D	1983	*McPhee* [1984]
MIZEX 84	east Greenland shelf	M	1984	*Muench et al.* [1986]
MIZEX 84	central YP	D	1984	*Morison et al.* [1987]
			1984	*McPhee* [1988]
AEDB	Nansen Basin and YP transect	D	1987	*Plueddemann* [this issue]
CEAREX O camp	NW slope of YP	D	1989	*Padman and Dillon* [1991]
CEAREX A camp	Fram Strait	D	1989	*Muench et al.* [1992]
CEAREX remote	NW slope of YP	D	1989	*Muench et al.* [1992]

*Mooring types are "drifting" (D) and "moored" (M).

CEAREX O camp. The O camp was heavily instrumented for physical oceanographic studies [see *Padman et al.*, 1991]. For this study we consider vertical profiles of hydrography and currents in the upper 350 m. As described by *Padman and Dillon* [1991], about 1500 profiles of temperature T, salinity S, and turbulent kinetic energy dissipation rate ε were obtained from March 31 to April 24, 1989. These profiles typically spanned most of the upper layer density stratification and the subsurface warm core of Atlantic Water. A 20-day period in which at least one profile per hour was obtained was used in this study to describe the diurnal hydrographic variability. Current profiles were measured with a 161-kHz, coded-pulse, acoustic Doppler current profiler (ADCP) [*Pinkel and Smith*, 1992] that was rigidly mounted to the ice. Unbiased estimates were obtained from about 20 m to 300 m. Hourly averages of currents are used for this study. The effective vertical resolution of the ADCP is about 12 m, much less than the vertical scale of the diurnal current, which was almost entirely barotropic (see section 3.2). Because the ADCP was rigidly mounted to the ice, whose orientation varied only very slowly over the drift track and was monitored, compass problems due to the locally weak geomagnetic field were minimized. The water depth was measured twice daily at the camp with a precision depth recorder operated by D. Farmer (Institute of Ocean Sciences, Sidney, British Columbia). Points marked "A," "B," "C," and "D" along the O camp drift track in Figure 1 represent significant features of the diurnal band variability near the YP and are discussed in detail in section 3.2.

CEAREX A camp. The A camp was instrumented with a Neil Brown "smart acoustic current meter" suspended at 35 m, and a Neil Brown ACM2 acoustic current meter at 150 m below the ice. Currents were sampled at 10-min intervals and then averaged to hourly values for the present analysis. Speed data are assumed to be accurate within the manufacturer's specifications of ± 0.01 m s^{-1}. Because the horizontal component of the Earth's magnetic field was locally weak, measurements of current direction were less reliable. Previous experience in the study region suggests that the directional error might be as great as 10°–20° (C. Darnall, NOAA Pacific Marine Environmental Laboratory, personal communication, 1990). Data were collected for the period March 31 to April 19, 1989 (year days 90–109).

Remote mooring. The remote mooring (RM) was instrumented in the same manner as the A camp. Data were recorded for the period April 1 to April 19, 1989 (year days 91–109). These data have been averaged to hourly values for the present study.

2.2. *Arctic Environmental Drifting Buoy*

The AEDB consisted of a surface float attached to a vertical mooring line supporting several different types of sensors [*Honjo et al.*, 1990]. Data were recorded internally and position was monitored by Argos satellite tracking. The AEDB was deployed on a multiyear ice floe at 86.12°N, 22.05°E on August 4, 1987. The buoy initially drifted toward the southwest, roughly along the Nansen Ridge, before turning to the southeast and crossing the Nansen Basin. After traveling nearly due east during mid-October, the buoy eventually turned back toward the southwest, and from November 1, 1987 (year day 305), to December 23, 1987 (year day 357), the AEDB was over the YP. The AEDB then moved rapidly through Fram Strait and into the Greenland Sea.

Upper ocean current profiles were measured with a 150-kHz, self-contained ADCP manufactured by RD Instruments. The ADCP emitted pulsed transmissions with a duration of 0.024 s at 1-s intervals for a period of 40 s. Each transmission sequence was repeated at 30-min intervals. Data were processed in forty 7.5-m depth cells, with the first cell being centered at 35 m, or 19 m below the transducers. Further details of the data processing are given by *Honjo et al.* [1990] and *Plueddemann* [this issue]. The same directional uncertainty due to the weak geomagnetic field as discussed for the A camp in section 2.1 applies to these data. The velocity data presented here were corrected for instrument motion with drift velocities computed from Argos position fixes (about 20 per day), using the method of *McPhee* [1988] (see section 2.1). Points marked "A," "B," "C," and "D," along the AEDB drift track in Figure 1 represent significant features of the diurnal band variability near the YP and are discussed in detail in section 3.2.

2.3. *Other Data Sources*

The permanent ice cover in the immediate region of the YP has prevented the deployment of fixed moorings that would be able to provide the necessary Eulerian time series for the separation of different diurnal tidal constituents. There have, however, been several long-term moorings in Fram Strait and also near the shelf break to the east of the YP, all of which provide useful regional information on diurnal currents. In addition, two ship drifts in the marginal ice zone (MIZ) over the southern YP are useful for describing the diurnal currents of the relatively shallow (<700 m) central plateau. Since the original impetus for the studies of diurnal amplification over the YP were current measurements from the Fram III and Fram IV drifting ice camps, we also briefly describe these experiments.

MIZEX 83 ship drift. During the 1983 Marginal Ice Zone Experiment (MIZEX 83) the icebreaker *Polarbjørn* drifted with the pack ice over the lower central Yermak Plateau for approximately 10 days [*McPhee*, 1984]. Unlike the CEAREX camps, which exhibited little ice motion at tidal frequencies, the *Polarbjørn* track indicated diurnal ice motion of up to 0.2 m s^{-1}.

MIZEX 84 ship drift. During MIZEX 84 the icebreaker *Polarqueen* drifted with the pack ice over the lower central Yermak Plateau for approximately 10 days, then was repositioned and drifted for a further 30 days [*McPhee*, 1988]. As with the *Polarbjørn* drift of 1983, tidal motions of up to 0.2 m s^{-1} were measured. *Morison et al.* [1987] present data from a profiling current meter which indicate that the subsurface currents also had a strong diurnal component, although there is significant shear at times through the upper 50 m (the mixed layer).

YMER moorings. Two moorings, each with three current meters, were deployed by the Swedish icebreaker *Ymer* on the continental slope north of the Barents Sea during the summer of 1980 [*Aagaard*, 1989]. The locations are approximately (81.5°N, 22.5°E) and (82.2°N, 45°E), in water depths of 460 and 1130 m, respectively. Tidal band spectra for the near-surface and deep currents at each site were kindly provided to us by K. Aagaard (personal communication, 1990).

Kvitøya mooring. A mooring consisting of two current meters (75 and 255 m deep) on a subsurface buoy was deployed in about 260 m of water from July 1980 to August 1981, between Kvitøya and Nordaustlandet, near the northern edge of the Barents Sea [*Aagaard et al.*, 1983].

MIZEX 83 moorings. A four-mooring array of current meters was deployed for about 40 days in June–July 1983 in about 2400 m of water in central Fram Strait [*Hunkins*, 1984]. The array was centered at approximately 78.5°N, 2°E.

MIZEX 84 moorings. Two current meter moorings were deployed from June 1984 to July 1985, at (78.73°N, 4.85°W) and (78.486°N, 4.55°W), on the east Greenland shelf [*Muench et al.*, 1986]. The water depth in each case was about 1000 m, and the current meters were at nominal depths of 100 and 400 m on each mooring.

Fram III and Fram IV. Fram III (1981) and Fram IV (1982) were manned ice camps that started in the Nansen Basin and drifted approximately southward onto the NW slope of the YP [*Johnson*, 1983; *Hunkins*, 1986]. Current meter data from several depths beneath each of these camps provided the first clear indication of strong diurnal tides in this region [see *Hunkins*, 1986, Figure 4].

3. Description of Tidal Variability

The Fram III and Fram IV current measurements presented by *Hunkins* [1986] indicated a clear difference in character between the weak diurnal currents away from the YP and stronger currents over the slope and plateau. We therefore review the diurnal variability with this partition in mind, looking first at the deep water and far-field measurements, then at the diurnal varibility over and near the YP.

Standard tidal analysis techniques can be used to determine the diurnal tidal band currents from fixed moorings, including separation of the principal tidal components from sufficiently long records. In measurements from drifting stations, however, both the amplitude and phase of a specific tidal component may vary through the record as the station drifts through different tidal regimes. For these records we estimate the diurnal band current (or isopycnal depth) by a process similar to the *McPhee* [1988] complex demodulation method for smoothing satellite navigation data (see section 2.1). At each time t for which data is available, a multivariate least squares fit is applied to data in the range $t \pm 0.5$ days. A measurement Y at time t is modeled by the sum of a mean and diurnal and semidiurnal sine waves with arbitrary phase,

$$Y(t) = \bar{Y} + a_d \cos(\omega_d t - \phi_d) + a_{sd} \cos(\omega_{sd} t - \phi_{sd})$$

where ω_d and ω_{sd} are the frequencies corresponding to waves of period 1 and 0.5 days, respectively. The "diurnal band" signal is then the reconstructed signal

$$Y_d(t) = a_d \cos(\omega_d t - \phi_d)$$

This technique allows for modulation of the diurnal band signal on a time-scale of about 1 day, the length of record used in the least squares fit.

3.1. *Deep Water and Far-Field Observations*

Moorings. Data from the MIZEX 83 mooring array in central Fram Strait to the west of Spitsbergen showed that the diurnal band currents were oriented predominantly north-south, i.e. along the axis of the strait [*Hunkins*, 1984]. The diurnal band current speeds were about 0.02 m s^{-1} and did not vary significantly with depth or between the different moorings. The two MIZEX 84 moorings on the east Greenland shelf [*Muench et al.*, 1986] were each in about 1000 m of water. Diurnal currents at both sites and all depths were less than 0.02 m s^{-1} for the K_1 component [*Muench et al.*, 1986], and were oriented approximately parallel to the local topography.

The three moorings on the northern slope of the Barents Sea, to the east of the YP, indicated that diurnal band currents were typically weak there also, being generally less than 0.02 m s^{-1}. The exception was the near-bottom current meter at the deeper (western) YMER mooring, where the rms diurnal band current was about 0.05 m s^{-1}, with most energy in the alongslope direction (K. Aagaard, personal communication, 1990).

In the cases for which individual tidal constituents are available, the MIZEX 84 moorings on the east Greenland slope and the Kvitøya mooring, both the O_1 and K_1 tidal components contributed significantly to the total diurnal band variability, the semimajor axis amplitude for K_1 being roughly twice as large as that for O_1. Other diurnal constituents such as P_1 were negligible. The interaction of the two principal diurnal tidal lines produces a spring-neap cycle with a period of about 13.6 days. For the purposes of the present paper, the important idea to retain is that observed diurnal band currents vary in time, even at fixed moorings.

Drifting camps over deep water. The moorings discussed above are located either on the continental slope or in the relatively shallow water of central Fram Strait. Several of the ice camps, however, drifted over the deep water surrounding the YP (Figure 1). In particular, the AEDB spent several weeks over the Nansen Basin to the north of the YP, while the CEAREX A camp remained offshore of the 3000-m isobath in northern Fram Strait for its entire measurement period.

The diurnal band currents for the A camp (Figure 2*a*) and the AEDB (Figure 3) over deep water had rms amplitudes of about 0.02 m s^{-1}, comparable to tidal analyses of mooring data (see above). The AEDB record over deep water was also modulated as expected from the superposition of the various tidal components. A numerical model of the K_1 tidal current along the drift track of the AEDB over the Nansen Basin (B. Gjevik, personal communication, 1991) suggests that the phase and amplitude of the K_1 tide is relatively constant in this region. Assuming this to be true also for the O_1 component, the along-track currents can be analyzed in the same way as measurements from an Eulerian mooring. A least squares fit of O_1 and K_1 frequencies to the deepwater AEDB record between days 277 and 294.2 (two spring-neap cycles) indicated that the semimajor axis currents for each component were similar, about 0.007 m s^{-1}. The slight difference in amplitude and ellipse orientation results in a ratio of spring-to-neap current magnitudes of about 6:1.

For the A camp, this type of spectral separation is precluded because of rapid variations of amplitude and phase coefficients for individual tidal lines in proximity to the slope. While Figure 2*a* indicates that significant modulation occurred, it is unlikely that the temporal and spatial variability could be separated without an effective tidal model of the region. Nevertheless, the A camp measurements do show that in deep water in Fram Strait, rms diurnal band currents

are about 0.02 m s^{-1}, with maximum diurnal-band currents of about 0.05 m s^{-1}.

It is clear from this review that the enhancement of diurnal band currents seen by *Hunkins* [1986] is a very localized phenomenon near the YP. The observations from the drifting stations also indicate that the decay scale of current amplification away from the YP is very short, with currents at both the CEAREX A camp and the AEDB being weak within 50 km of the bottom of the plateau slope.

3.2. *Observations on the Yermak Slope and Plateau*

Fram III and Fram IV. Current meters below the mixed layer in both Fram III and Fram IV revealed stronger diurnal band currents when the camps approached the upper slope of the YP [see *Hunkins*, 1986, Figure 4]. The maximum amplitude of the diurnal currents measured from Fram III was about 0.12 m s^{-1}. Fram III remained near the 1000-m isobath for several days, during which time the tidal current regime changed from being predominantly diurnal to semidiurnal. We interpret this to mean that the diurnal band currents were modulated by more than simply changing bathymetry, with the most likely candidate being the spring-neap cycling by superposition of O_1 and K_1 tidal waves.

Fram IV followed a drift track which only briefly approached the central slope of the YP (minimum water depth of about 2000 m). Nevertheless, strong diurnal currents with amplitudes up to 0.15 m s^{-1} were found, commencing from the camp's first approach to the lower slope and being largest on the central slope.

CEAREX O camp. Currents measured by the ADCP at the O camp for vertical averaging bins centered at 35 m (the surface mixed layer), 150 m (the peak density gradient), and 250 m (the Atlantic layer core) are shown in Figures 4*a* and 4*b* for the cross-slope (150°T) and along-slope (60°T) components, respectively. There was little change in amplitude, and no measurable phase shift, with changing depth. A

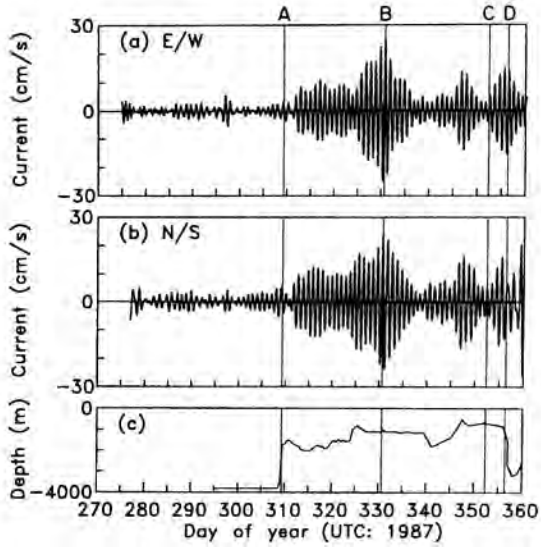

Fig. 3. Diurnal band current variability from the Arctic environmental drifting buoy (AEDB). (*a*) East-west 150-m current, (*b*) north-south 150-m current, and (*c*) water depth. Vertical reference lines marked "A," "B," "C," and "D" are discussed in the text.

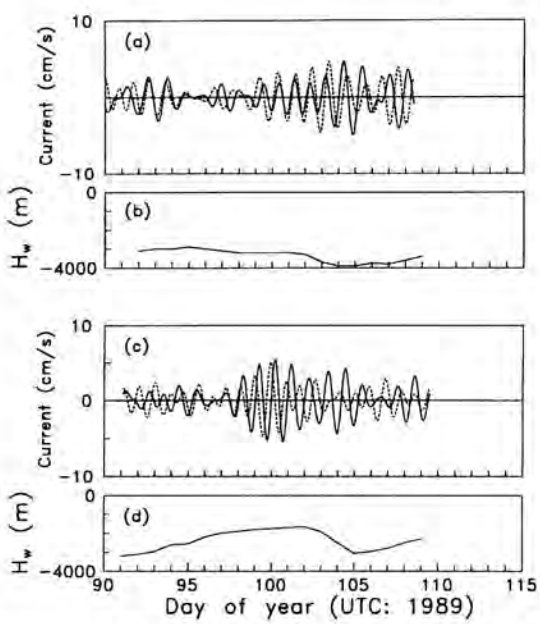

Fig. 2. Diurnal band current variability at the CEAREX A camp and the remote mooring. (*a*) A camp east-west 150-m current (solid) and north-south 150-m current (dashed), (*b*) A camp water depth, (*c*) remote mooring east-west 150-m current (solid) and north-south 150-m current (dashed), and (*d*) remote mooring water depth.

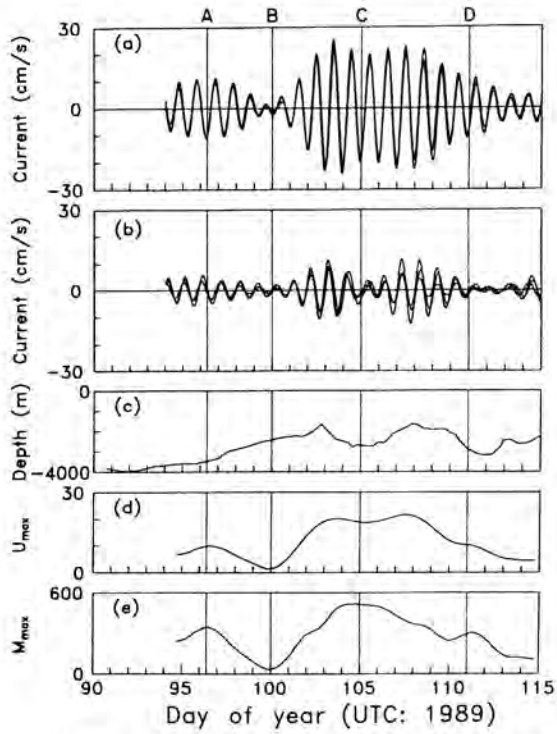

Fig. 4. Diurnal band current variability at the CEAREX O camp. (*a*) cross slope currents at 35-, 150-, and 250-m depth; (*b*) along-slope currents at 35-, 150-, and 250-m depth; (*c*) water depth; (*d*) cross-slope diurnal current amplitude U_{max} (centimeters per second), and (*e*) cross-slope maximum diurnal-band mass flux, M_{max} (square meters per second). Vertical reference lines marked "A," "B," "C," and "D" are discussed in the text.

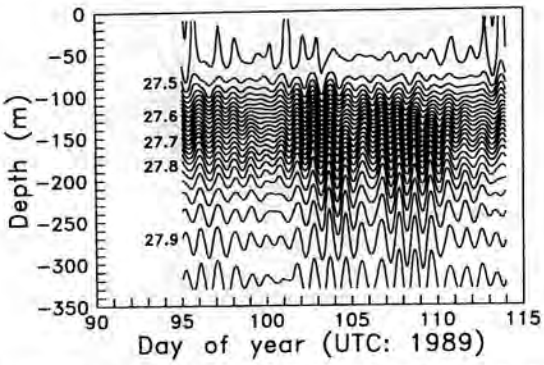

Fig. 5. Transect of potential density σ_θ during the CEAREX O camp drift. Data have been filtered to remove frequencies greater than 1/18 cycles per hour.

similar result was found for the AEDB data whenever the diurnal band currents were large relative to the typical deepwater values of about 0.02 m s^{-1}. For the remainder of this paper we will concentrate on data from 150-m depth, which was common to most sites and was below the surface stress layer. The largest measured diurnal band current at the O camp was about 0.24 m s^{-1} near year days 103 and 107.

We have shown in Figure 4 four points corresponding to distinctive features along the drift track (Figure 1). Point A was a local maximum in diurnal band current, just as the O camp first approached the plateau slope. Point B was a local current minimum, while point C corresponded to the local maximum offslope excursion of the camp during a period of strong westward wind stress. This was also close to the time of maximum cross-slope tidal mass flux (see Figure 4*e*). Point D indicates the location of an ellipticity maximum (see section 5 and Figure 11). The observed modulation of the diurnal currents throughout the drift cannot, however, be unambiguously separated into spatial and temporal variability. There is evidence, for example, of topographic modulation near point C; however the currents were larger over deep water (point A) than over the lower slope. This suggests that at least part of the observed modulation was related to spring-neap cycling rather than topographic effects. The period of the spring-neap cycle, 13.62 days, is comparable to the length of time spent by the camp over the plateau slope.

We hypothesize that point C denotes a maximum in the spring-neap cycle, even though higher currents were found near days 103 and 107 when the camp was in shallower water upslope. Assuming that the uniform velocity in the upper 300 m extends to the seabed, the cross-slope, depth-integrated volume flux corresponding to the peak cross-slope current (U_{max}) can be estimated as

$$M_{max} = H_w U_{max} \tag{1}$$

Figures 4*d* and 4*e* show U_{max} and M_{max}. The maximum cross-slope current amplitude at each time t is determined from the amplitude of a cosine wave fitted (in the least squares sense) to data in the range $t \pm 0.5$ days. The volume flux M_{max} peaks during the camp's local maximum offslope excursion near point C.

Diurnal variability was also found in the hydrographic properties (Figure 5). The vertical displacement of isopycnals increased approximately linearly with depth and was modulated in time, in phase with variations of the cross-slope tidal current. Note that such large isopycnal displacements impose severe constraints on the use of nonaveraged density profiles for determining geostrophic velocities in this region.

CEAREX remote mooring. The RM drift track (Figure 1) was qualitatively similar to that of the O camp. The initially southward, upslope motion was followed by wind-forced advection toward the west, after which the RM drifted roughly southward in the Transpolar Drift. The shallowest isobath (Figures 1 and 2*d*) crossed by the RM during the experiment was about 1600 m, similar to the shallowest isobath crossed by the O camp. Maximum currents (Figure 2*c*) were about 0.05 m s^{-1} near $t \approx 100.0$, which was the approximate time of minimum currents at the O camp. At this time, however, the RM was in relatively shallow water (1600 m), where diurnal currents are expected to be relatively strong. We propose that the currents observed by the RM at this time represent the topographic amplification of neap tidal forcing whereas the maximum currents at the O camp at $t \approx 107$ are due to amplification of spring tidal forcing. The implied spring-neap tidal ratio of about 5:1 over the upper slope (0.25 m s^{-1} at $t = 107$ at O camp versus 0.05 m s^{-1} at $t = 100$ at the RM), is comparable to the modulation found in the deepwater segment of the AEDB tidal current data (see section 3.1). If O_1 and K_1 are indeed the principal diurnal tidal current components in this region, the large spring-neap tidal ratio implies that the amplitudes of these two tidal coefficients must be comparable, at least on the western slope of the YP.

Arctic environmental drifting buoy. The water depth under the AEDB for the period of interest is shown in Figure 3*c*. Water depths are taken from *Jackson et al.* [1984]. The amplitudes of both east and north components of diurnal current (Figures 3*a* and 3*b*) were clearly correlated with water depth. As was discussed above, however, the current amplitudes over deep water were also modulated, with O_1 and K_1 components being approximately equal. There was also a local minimum current as the AEDB crossed the central YP, suggesting that the maximum currents were focused on the upper slope rather than continuing across the central plateau.

The largest measured currents were about 0.25 m s^{-1} near day 331, while the AEDB was roughly following the 1000-m isobath southward. These current speeds were similar to the maximum values at the O camp. Several reference points from the AEDB drift track (Figure 1) are shown in Figure 3 (and repeated in Figure 12). Point A corresponds to the AEDB's first contact with the plateau slope, point B is the location of largest diurnal currents, point C indicates where the AEDB crossed the shallow center of the plateau, and point D shows where the AEDB left the plateau on the western (Fram Strait) side.

MIZEX 83 and MIZEX 84 ship drifts. The satellite-tracked drift paths of the *Polarbjørn* and *Polarqueen* provide the most comprehensive data sets over the central Yermak Plateau. We are, however, unable to determine quantitatively how the ice drift in the marginal ice zone is coupled to the local tidal forcing. We hypothesize that the ice responds to the diurnal band current integrated over an area comparable to the coherence scale of ice compactness. In the

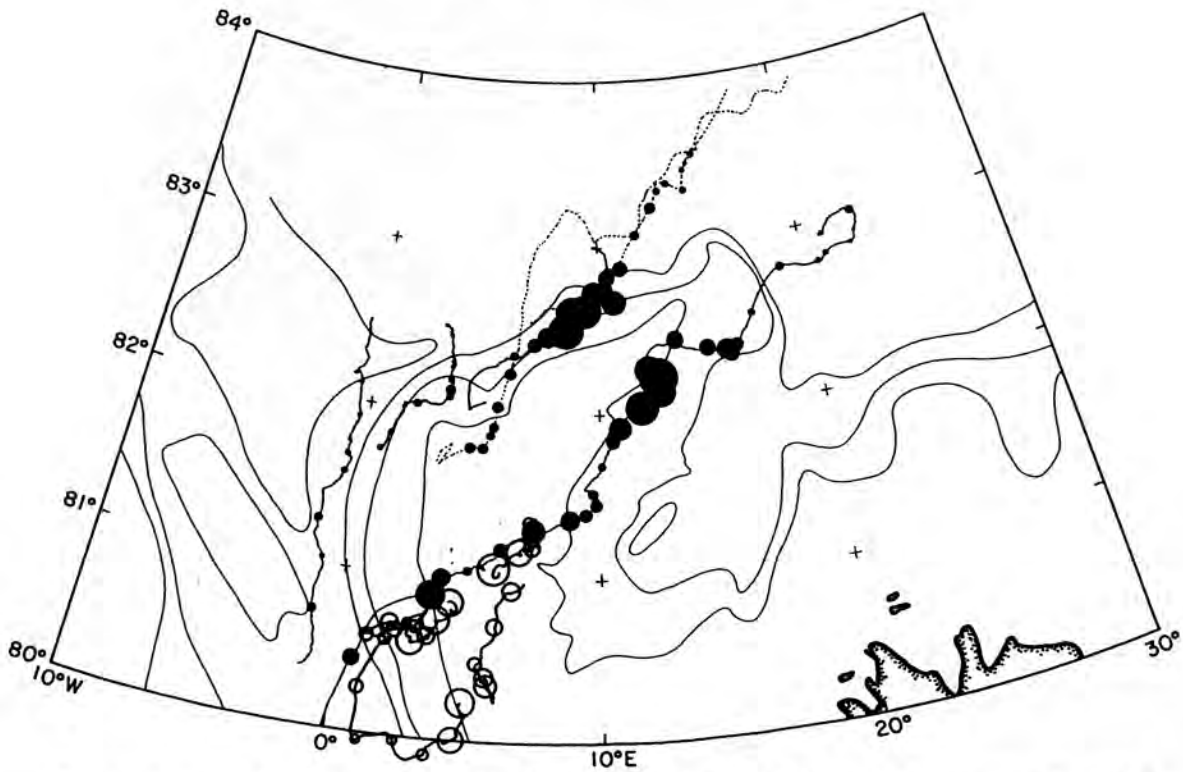

Fig. 6. Summary of tidal current observations from drifting stations. Symbols are plotted approximately every 2 days along each track, with the radius being proportional to the semimajor axis of the local diurnal tidal ellipse. Solid circles are based on analyses of measured currents, while open circles represent currents derived from satellite-tracked ice motion (MIZEX 83 and MIZEX 84 ship tracks).

marginal ice zone this scale may be 1–10 km, while further north and in winter the coherence scale may be greater than 100 km, effectively decoupling ice motion from the local tidal current, which is assumed to be modulated over distances comparable to the topographic length scales. The interpretation of satellite-tracked buoys [*Hoffman*, 1990; *Prazuck*, 1991] and ship drift tracks (this paper) in terms of the spatial structure of barotropic diurnal currents is therefore extremely difficult. Even within a single drift track, such as the second section of the *Polarqueen* drift in 1984, the ice compactness might vary substantially between the central plateau, the slope, and the surrounding deep water. If this is the case, much of the observed current amplitude modulation may simply be due to the variable ice conditions. Interpretation becomes even more difficult if the ice compactness is related to the divergence of the underlying diurnal tides (see section 6), in which case the maximum tidal band ice velocities might actually be found in the region of maximum tidal stress divergence rather than at the location of maximum tidal currents. With these caveats in mind, however, we have included the MIZEX 83 and MIZEX 84 ship drift velocities in the summary of diurnal current observations.

3.3. *Summary of Diurnal Tidal Observations*

The diurnal band current amplitudes in the region of the YP vary owing to both spatially dependent amplification and temporal modulation from superposition of different tidal components. The largest currents were found on the upper slope during periods of spring tides (O_1 and K_1 approximately in phase), and there is evidence from the AEDB that currents decayed from there to the relatively shallow core of the plateau. The observed amplitudes of the diurnal tidal currents are illustrated in Figure 6, where the radii of the plotted symbols represent the measured semimajor axis current approximately every 2 days along the various drift tracks. Solid symbols represent measured absolute currents, whereas open circles indicate that the currents are based on measured ice motion. The separation of weak flow in the surrounding deep basins from amplified flow over the slope is clear. There is conflicting evidence, however, from the AEDB and the MIZEX ship drift data as to whether the currents over the central plateau are significantly less than those over the upper slope. We also do not, at this time, know how the compactness of the ice cover and its associated variation in frictional damping might affect the dynamics of the diurnal tidal flow in this region.

4. MODELS OF TOPOGRAPHIC AMPLIFICATION OF DIURNAL TIDES

4.1. *Cross-Slope Mass Conservation*

The simplest conceptual model of topographic current amplification is to assume that the plateau does not affect the depth-integrated mass flux associated with the propagation of the basin-scale barotropic Kelvin tidal waves. With this assumption, the cross-slope tidal current amplitude $|u_x|$ in water of total depth H_w is

$$|u_x| = |u_{x,d}| \frac{H_d}{H_w} \tag{2}$$

where $|u_{x,d}|$ and H_d are the cross-slope current amplitude and the water depth in the deep basin surrounding the plateau, respectively. From (2), the strongest currents are predicted to occur over the shallowest water of the central plateau. This is consistent with the results of a fine-grid numerical model of K_1 tides described by *Gjevik* [1990] and *Gjevik and Straume* [1989]; however, their predicted tidal currents were much less than have been observed.

4.2. *Near-Resonant Shelf Waves Around an Axisymmetric Plateau*

This model for diurnal current amplification was first proposed by *Hunkins* [1986], then was developed for a plausible parameterization of forcing and friction by *Chapman* [1989]. The interested reader is referred to Chapman's paper for complete details. The model assumes that an axisymmetric wave mode can propagate completely around the plateau with near-resonant forcing by a large-scale, barotropic, rectilinear Kelvin wave. The amplitude is a function of (1) the difference between the forcing frequency and the plateau's resonant frequency, and (2) frictional damping. Resonance relies on the path length of the free wave around the plateau's perimeter being near to an integral number of wavelengths. Friction is introduced as benthic stress, although stress at the ice-water interface should also be included for a rigid ice pack. Chapman obtained amplification estimates that were roughly consistent with the observed ratio of diurnal band currents over the slope and deep water. Nevertheless, as a glance at the plateau geometry in Figure 1 shows, the YP is far from axisymmetric, so this approximate agreement between Chapman's model and observations is somewhat surprising.

4.3. *Shelf Waves on a Long, Straight Escarpment*

The observations discussed in section 3 suggest that below the surface stress layer, diurnal currents are principally barotropic. These observations are reminiscent of the diurnal barotropic shelf waves studied by *Middleton et al.* [1987] in the southern Weddell Sea. Because of the short cross-slope scale compared with the width of the relatively flat central plateau, we follow Middleton et al. by using the *Saint-Guily* [1976] model of divergent barotropic flow due to the continental slope. Note that the Saint-Guily model applied to the YP was considered independently by *Prazuck* [1991] in order to qualitatively assess the importance of isobath curvature on the propagation of the topographic waves.

We first assess the validity of the barotropic assumption by evaluating the Burger number S along the sloping bottom,

$$S = \left(\frac{N}{f}\right)\frac{dH_w}{dx} \tag{3}$$

where N is the buoyancy frequency, f is the local Coriolis frequency, and dH_w/dx is the bottom slope. *Chapman and Hendershott* [1982] indicate that for $S < 0.2$ everywhere on the seabed, barotropic shelf wave models are quantitatively correct. During the O camp drift, hydrographic properties were measured only in the upper ocean (Figure 7), so that N near the seabed must be estimated from an extrapolation of the decay of the buoyancy frequency profile. At 700 m, the approximate shallowest water depth on the plateau slope,

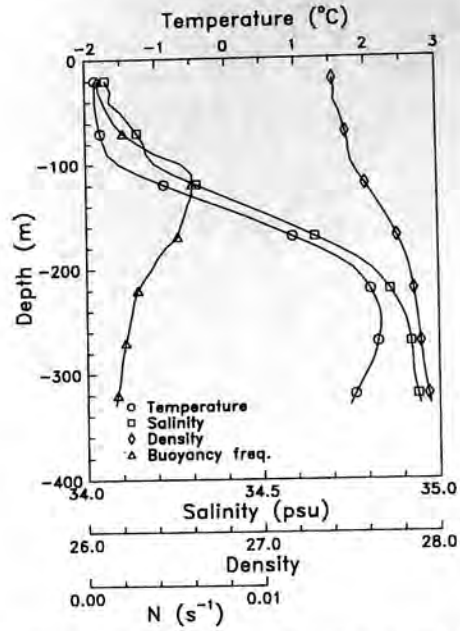

Fig. 7. Mean profile of temperature T, salinity S, potential density σ_θ, and buoyancy frequency N, from 20 to 320 m during the CEAREX O camp drift.

the estimated value of N is less than 0.001 s^{-1} and the bottom slope is about 0.05, giving $S \approx 0.3$. This suggests that there may be some baroclinic structure to the shelf waves; however, in the ADCP data from both the O camp and the AEDB the diurnal currents are independent of depth, at least in the upper 300 m. D. Chapman (personal communication, 1991) has noted that our observations from the upper 350 m are insufficient to determine whether the barotropic assumption is appropriate. To test this assumption, we ran *Brink and Chapman*'s [1987] numerical model of baroclinic shelf waves for the topography and estimated stratification appropriate to the northwest slope of the YP and found that the current amplitude changed by less than 20% throughout the water column. Given the other approximations of the model and the uncertainty of the estimate of N near the bottom, the barotropic assumption appears to be a reasonable working hypothesis for the present study.

At first glance, the large diurnal band isopycnal displacements at the CEAREX O camp (Figure 5) appear to be inconsistent with the barotropic assumption. Consider, however, a horizontally homogeneous, vertically stratified ocean, with isopycnals intersecting the bottom topography. As a current that is uniform with depth flows up the slope, the flow accelerates (by continuity), and isopycnals converge. The isopycnal adjacent to the seabed is raised vertically by the product of the horizontal distance and the bottom slope, while the height of the free surface barely changes. From shelf-wave models at low S, the decay in vertical motion is almost linear from the seabed to approximately zero at the sea surface. In Figure 5 we find that linearly extrapolating isopycnal displacements from our measurements in the upper 350 m to the seabed in 2000 m of water during spring tides results in a peak-to-peak isopycnal displacement at the seabed of about 300 m. This is consistent with a cross-slope diurnal current amplitude of about 0.2 m s^{-1} (as observed) flowing over the estimated bottom slope of

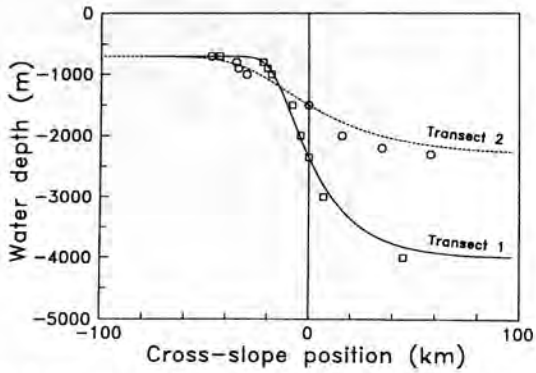

Fig. 8. Cross-slope bathymetry for transects 1 (north-west slope) and 2 (east slope) of the Yermak Plateau (see Figure 1). Also shown is the least-squares-fitted Saint-Guily topography (equation (4)), using the values of H_0, a_0, and λ given in Table 2.

$\partial H_w/\partial x \approx 0.05$ for one half of a diurnal tidal cycle. These results support the view that the diurnal band isopycnal fluctuations are driven primarily by the vertical motion induced by the cross-slope, barotropic flow across the sloping bottom. There was, however, also a cross-slope horizontal density gradient [*Muench et al.*, 1992] that would have been advected past the O camp by the cross-slope diurnal currents, contaminating the measurement of true vertical motion to some extent.

The Saint-Guily model expresses the cross-slope topography as the pair of transformations

$$q = 1 + \lambda \tanh z \tag{4a}$$

$$y' = z + \lambda \ln(\cosh z) \tag{4b}$$

where $q = H_w/H_0$ is a dimensionless depth, $y' = y/a_0$ is the dimensionless cross-slope coordinate, H_0 and a_0 are the scale depth and horizontal slope scale width, respectively, and λ is the slope parameter. Model sections are generated by allowing z to vary between $+\infty$ and $-\infty$. Two sections across the YP (Figure 1) are shown in Figure 8, with the least-squares-fitted model shelves. It can be seen that H_0 is the central depth on the slope and a_0 is approximately the horizontal distance from this point to the top of the slope. The slope parameter λ is given by

$$\lambda = \frac{H_d - H_s}{H_d + H_s} \tag{5}$$

where H_d and H_s are the offshore (deep) and shelf (shallow) water depths, respectively. For a fixed central plateau water depth, therefore, λ is a function only of the offshore water depth, H_d.

5. Comparison of Observations With Models

The cross-slope transects shown in Figure 8 represent the northwest slope sampled during CEAREX and the eastern slope sampled by the AEDB. The values of H_0, a_0, and λ for the least-squares-fitted profiles for these transects are given in Table 2. The dispersion curves for the *Saint-Guily* [1976] model (Figure 9) are functions of λ only, and the bold curves in Figure 9 correspond approximately to the values of λ for the two transects in Figure 8. The frequencies of the two principal diurnal tides are also indicated. A logarithmic scale

TABLE 2. Comparison of Parameters for Cross-Slope Transects Fitted to the *Saint-Guily* [1976] Model Topography

Variable	Transect 1	Transect 2
H_d, m	4000	2300
H_0, m	2350	1500
α_0, km	22.5	40.0
λ	0.70	0.53
k_2 [O_1, K_1], 10^{-5} m^{-1}	[4.3, 3.5]	[1.1, 0.4]
c_p [O_1, K_1], m s^{-1}	[1.6, 2.1]	[6.2, 18.2]
c_g[O_1, K_1], m s^{-1}	[−0.5, −0.6]	[−0.9, ~0]

Transects 1 and 2 represent the NW slope sampled during CEAREX, and the eastern slope sampled by the AEDB, respectively (see Figure 1 for transect locations and the text for parameter definitions). Dispersion characteristics are listed for the negative group velocity (short wavelength) waves only.

is used for alongslope wavenumber because of the wide scale separation of the two wavenumber roots for each diurnal wave frequency. For sufficiently small λ, neither diurnal constituent exists as a free wave mode. On the eastern slope, K_1 is only marginally supported, and the group velocity, $c_g = \partial\omega/\partial k$, is approximately zero. If the diurnal tide is locally amplified by the periodic forcing of the background Kelvin wave, the energy can only slowly radiate away from this site. On the NW slope, however, both K_1 and O_1 waves can exist and propagate freely. We note for the moment that the variation in free wave propagation characteristics around the plateau is not consistent with the simple axisymmetric models.

The phase of barotropic shelf waves necessarily propagates with the shallower water to the right (in the northern hemisphere). The energy (and group velocity) of such waves can, however, propagate in either direction. For the O_1 component on the eastern slope and for both components on the NW slope, both positive and negative group velocities are possible, even when the effects of weak stratification are included. The positive root k_1 is at very small wavenumbers, corresponding to length scales much larger than the plateau scale. The negative root k_2 corresponds to along-slope wavelengths of O(100 km), although this value is quite sensitive to both wave frequency and slope parameter.

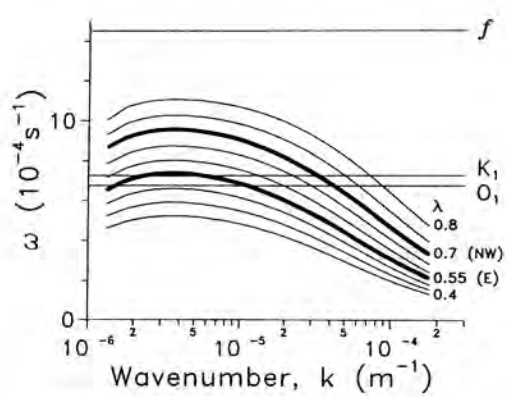

Fig. 9. Dispersion curves for shelf waves for a range of the slope parameter, λ, using the *Saint-Guily* [1976] model for a broad, flat shelf. Lines labelled (NW) and (E) are approximations of the northwest and east slopes of the Yermak Plateau, respectively (see Table 2). The along-slope wavenumber k is plotted on a logarithmic scale. Also shown are the frequencies of the inertial (f) and the O_1 and K_1 diurnal tidal components.

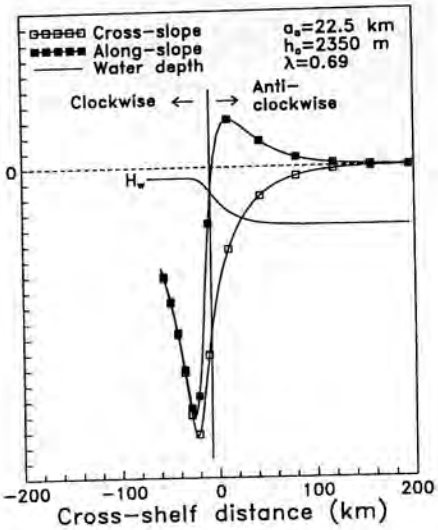

Fig. 10. Structure of cross-slope and along-slope currents for the large-wavenumber root of an O_1 barotropic shelf wave over the idealized topography of the northwest slope of the Yermak Plateau, following *Saint-Guily* [1976]. The current ellipse is approximately circular and anticlockwise in deep water (right-hand side), circular and clockwise over the plateau (left-hand side), and rectilinear oriented cross-slope at middepth over the slope.

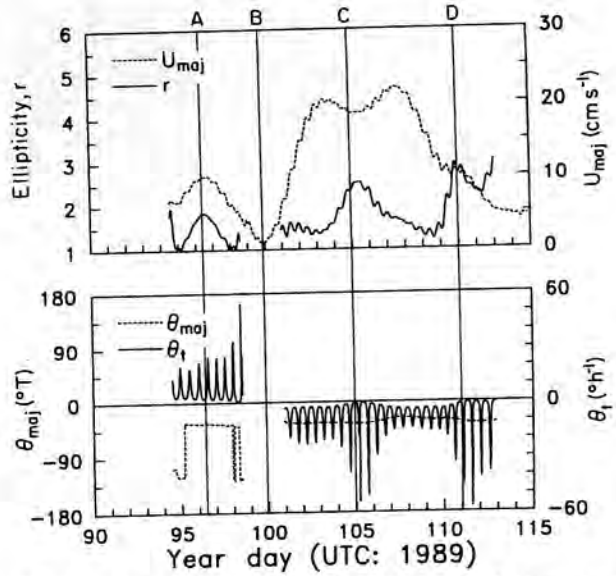

Fig. 11. O camp diurnal-band ellipse properties for currents at 150-m depth. (*a*) Semimajor axis current magnitude U_{maj} and ellipticity r. (*b*) Ellipse orientation θ_{maj} and ellipse rotation rate θ_t.

Middleton et al. [1987] found evidence of this short-wavelength mode from coherences between elements of an along-slope array in the southern Weddell Sea, and no evidence of the positive group velocity mode (J. Middleton, personal communication, 1990). The phase speed of the latter mode, however, is so great that coherence estimates would suggest an in-phase oscillation throughout the array, indistinguishable from the deepwater Kelvin mode.

For a typical value of the slope parameter for the NW slope, $\lambda = 0.7$, the cross-slope structure of the K_1 barotropic shelf wave currents for the short wave ($c_g c_p < 0$) is shown in Figure 10. The cross-slope and along-slope currents are always 90° out of phase, so that the rotation sense and ellipticity can be determined solely from the magnitude and sign of the two components. The current magnitude is largest over the slope, with an approximately exponential decrease toward deep water and across the shelf (or plateau). The current ellipse is approximately circular over the lower slope and the velocity vector rotates anticlockwise. Near the central slope, the flow is rectilinear and cross-slope. Maximum currents are found at the top of the slope, where the current ellipse is again circular but rotates clockwise.

These basic diagnostics allow us to investigate the possibility that the observed diurnal band currents can be explained by the barotropic shelf wave model, in the absence of simultaneous along-slope measurements such as those that were available to *Middleton et al.* [1987]. Figure 11 shows the ellipse orientation θ_{maj}, ellipticity r, semimajor axis magnitude U_{maj}, and ellipse angular velocity θ_t ($= \partial\theta/\partial t$), for the O camp measurements near and over the NW slope. Ellipse properties other than U_{maj} were not plotted when U_{maj} was less than 0.05 m s^{-1}, since the ellipse properties were generally unstable at these times. For most of the drift, θ_{maj} was about −30°, indicating predominantly cross-slope flow, a result which is consistent with the shelf wave model. The plot of θ_t shows a change of sign near t = 98.5. This indicates that the rotation sense was anticlockwise in the deeper water and was clockwise throughout the central, shallower, drift phase. Of considerable interest is the rapid increase in ellipticity near t = 105, when the camp drifted temporarily over slightly deeper water. The ellipse variability therefore also qualitatively supports the shelf wave model.

Diurnal currents at the A camp and the remote mooring rarely exceed our threshold of 0.05 m s^{-1}; therefore no attempt has been made to analyze their ellipse parameters. Nevertheless, these two data sets qualitatively agree with the model. Currents were largest at RM while the camp was over 1600 m of water, near t = 100 (Figure 4*c*). Maximum currents were, however, about 0.05 m s^{-1}, compared with 0.25 m s^{-1} while the O camp was in a similar water depth. There are appreciable differences between the cross-slope bathymetry at the two points where the O camp and the RM approached the plateau, which might explain some differences in measured currents between the two sites. An alternative explanation is that the RM drifted onto the slope during a temporal minimum ("neap") in shelf wave currents while the O camp was over the slope during maximum ("spring") currents. Currents at the RM at this time would therefore reflect the topographic amplification of the temporal minimum in forcing near day 100 (Figures 4*d* and 4*e*).

A similar analysis of ellipse properties for the AEDB data is shown in Figure 12. Note that the time base in Figure 12 is 60 days compared with only 25 days for Figure 11 (O camp). Again, ellipse parameters were not plotted when U_{maj} was less than 0.05 m s^{-1}. The very rapid change in water depth as the AEDB approached the YP (point A) precludes identification of the midslope depth at which ellipticity r should be high. However, as the AEDB left the plateau on the Fram Strait side near t = 357 (point D), r did indeed increase at midslope, and the rotation rate changed sign at the same time.

As was discussed above, the AEDB data provided a transect across the shallowest central portion of the plateau. At the central point (marked "C" in Figures 1, 3, and 12),

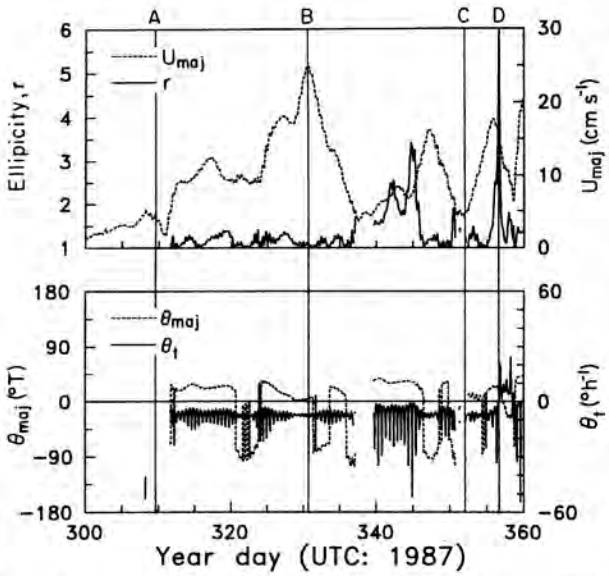

Fig. 12. AEDB diurnal band ellipse properties for currents at 150-m depth. (*a*) Semimajor axis current magnitude U_{maj} and ellipticity r. (*b*) Ellipse orientation θ_{maj} and ellipse rotation rate θ_t.

the current was locally weak, which is again consistent with the shelf wave model in which the current decays on the shallow side of the escarpment, but inconsistent with simple two-dimensional continuity arguments (equation (2)). The Arctic numerical tidal model of *Gjevik* [1990] and *Gjevik and Straume* [1989] predicted maximum currents over the shallow central plateau, possibly a result of the model's failure to resolve the cross-slope scales of the slope-trapped waves.

These results all support the hypothesis that the dominant components of diurnal variability over the northern section of the YP are propagating barotropic shelf waves. We have also suggested that the principal contribution is from relatively short waves in which the group velocity opposes the phase propagation, although the data base is inadequate to resolve this issue unambiguously. If the short waves are dominant, however, the oscillations seen on the NW slope would result from energy propagation from farther east. A further clue to the initiation of these short-wave shelf modes is provided by *Gjevik*'s [1990] Arctic tidal model for K_1. This model suggests that most of the K_1 energy flux into the Arctic from the North Atlantic occurs as a Kelvin wave trapped around the western and northern coasts of Spitsbergen, to the south of the Yermak Plateau. We hypothesize that this energy flux across the neck of the YP provides the necessary forcing for the generation of the short-wave modes. The proposed generation mechanism is similar to *Thomson and Crawford*'s [1982] initial proposal for the production of diurnal shelf wave modes along the west coast of Vancouver Island. These authors suggested that energy may be input at the point on the shelf where c_g is locally near zero, allowing maximum amplification, but with some topographically induced leakage in both directions. Assuming the validity of the Saint-Guily model, the eastern slope of the YP (transect 1) is near-resonant for K_1 waves. The O_1 waves will be near-resonant even further south on the eastern slope, where the "deepwater" depth (and consequently λ) are smaller. The aim here is not, however, to prove that a specific source has been identified, but rather to suggest that topographic variability around the YP may lead to processes that are totally excluded by existing axisymmetric models.

The high sensitivity of the shelf wave dispersion relationship to topographic variability around the YP implies that an adequate numerical model will require much better grid resolution than is presently used. For example, the relatively high resolution model of Arctic tidal currents by *Gjevik* [1990] used a 50-km bathymetric grid, whereas the cross-slope length scale on the northwest slope is about 25 km (Table 2). Gjevik's model employed a large horizontal diffusivity for numerical stability, resulting in maximum currents over the central portion of the YP rather than over the slope. Even when the grid resolution was improved to 25 km, maximum currents were still predicted over the central plateau (B. Gjevik, personal communication, 1991). Improved numerical models are justified, however, in view of the dynamical importance of diurnal currents in this region, as is discussed in section 6.

6. EFFECTS OF TIDES ON THE REGIONAL CIRCULATION AND HYDROGRAPHY

The amplified diurnal tide is the largest contributor to the total kinetic energy density near the YP. Although locally stronger currents may be associated with intermittent phenomena such as submesoscale eddies [*Muench et al.*, 1992], the time-averaged contribution of these intermittent features is expected to be small. Both the under-ice, surface mixed layer and the benthic mixed layer are expected to be sensitive to the presence of strong currents through the increased mean stress magnitudes occurring at these boundaries. In each case we expect that the layer thickness will be greater than in the absence of tidal currents (M. McPhee, personal communication, 1991). The map of mixed layer depth determined from the large-scale conductivity-temperature-depth (CTD) survey during CEAREX (Figure 13), shows that the mixed layer over the slope of the YP was indeed thicker than in the deep basin surrounding the plateau. The mixed layer was also thinner over the core of the YP, suggesting that surface stress might be smaller there than over the slope. This result is consistent with the weak currents measured by the AEDB over the plateau core (point C in Figures 5 and 12), but may also be due to continuous upwelling of the pycnocline if the large-scale surface velocity field over the YP is divergent.

Spatially variable tidal currents also lead to stress divergence on the base of the pack ice. Ice motion at diurnal frequencies during the CEAREX and AEDB programs was an order of magnitude weaker than the underlying currents. We believe that this is related to the compactness of the pack ice. We imagine that the ice floe to which each drifting station is coupled is a rigid sheet that has some characteristic horizontal scale, L_i, say. The diurnal ice motion is then the response to the tidal stress integrated over the entire sheet. If L_i is greater than the topographic scale over which the diurnal currents are assumed to be modulated, the result is a divergent stress applied to the ice base. In turn, this stress induces internal ice stresses and consequently causes ice ridging and lead formation. The potential importance of this tidally induced stress divergence can be evaluated by comparing its strength with the atmospheric stress divergence. Given an ice-water drag coefficient of about 0.006, appropriate to multiyear pack ice [*Johannessen*, 1970; *Langleben*,

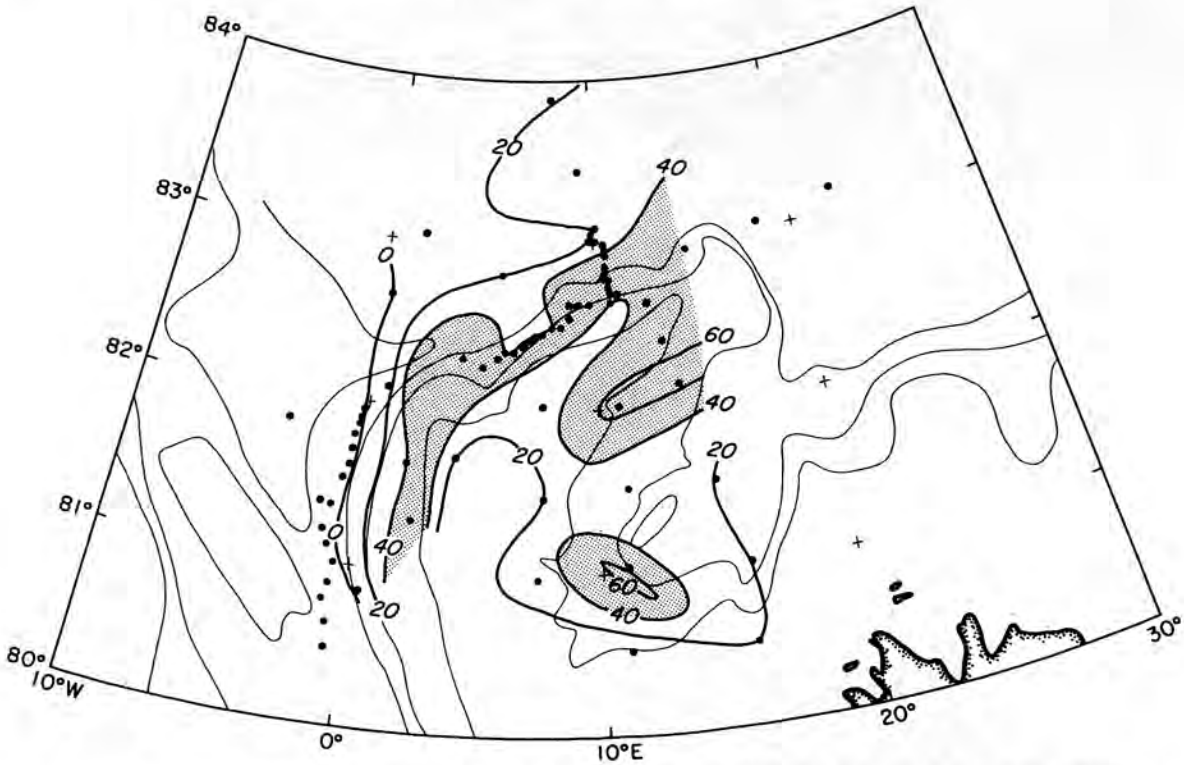

Fig. 13. Regional variation of mixed layer depth (in meters) during CEAREX. Regions where the mixed layer is thicker than 40 m are shaded. Dots represent station locations [see *Muench et al.*, 1992].

1980], a change of 0.2 m s^{-1} over the 50-km topographic scale results in a stress divergence of about 5×10^{-6} Pa m^{-1}. For an air-ice drag coefficient of 0.0015 and a typical wind velocity gradient of 10 m s^{-1} over 1000 km, the equivalent air-ice stress divergence is 2×10^{-7} Pa m^{-1}. That is, under typical conditions the tidal stress divergence on the underside of the ice is an order of magnitude greater than the wind stress divergence on the ice surface. Although the divergent stress loading by the tides is cyclic, we hypothesize that ridging and lead formation could be influenced by the amplified tide. We note that the satellite-tracked drifters that showed strong diurnal motion [*Hoffman*, 1990; *Prazuck*, 1991] were over the northwest slope of the YP during summer. These drifters underwent several diurnal loops with current speeds of up to 0.15 m s^{-1}, indicating that at least in summer, the coherence scale L_i of the ice pack is sufficiently small for the ice to be coupled to the local diurnal currents. We are unable at this time to determine whether the looser pack ice in summer in this region is due to the tidal stresses or is simply a response to atmospheric stress on the weakened summer ice pack.

While mixing at the upper and lower boundaries is likely to be enhanced, the impact of this mixing may be more on the dissipation of the tidal wave itself rather than affecting the general circulation. *Huthnance* [1981] has already discussed the loss of tidal energy as the tidal Kelvin wave propagates into the Nordic seas and Arctic Ocean. In particular, he attempted to quantify the increased frictional losses that result from tidal current amplification over the broad, shallow shelf of the Barents Sea. In the present study, however, we are more concerned with the possible effects on the large-scale hydrography and general circulation.

The ability of the tide to affect the hydrographic properties, such as the Atlantic Water core temperature and salinity, depends on its ability to create appreciable turbulence within the pycnocline. As was noted in section 3.2, the tidal flow is primarily barotropic, with little vertical shear for the initiation of the shear instabilities that are the expected conduit for mixing to microscales [*Gregg*, 1987]. Nevertheless, as *Padman and Dillon* [1991] and *Padman et al.* [1991] have demonstrated, the dissipation rate in the pycnocline has a strong diurnal component of variability. These previous studies have suggested that the tide is responsible in some manner for the production of high-frequency wave packets [*Czipott et al.*, 1991], which are then related to the occurrence of energetic mixing patches. *Padman and Dillon* [1991] estimated that the "mean" diapycnal heat flux was about 30 W m^{-2} above the Atlantic layer core when the tide was strongest, compared with less than 3 W m^{-2} in the deep water of the Nansen Basin near the YP. In the deep central Arctic Basin, well away from significant topographic features, the heat flux from the Atlantic layer may be less than 0.1 W m^{-2}, and then only due to the efficiency of double-diffusive processes [*Padman and Dillon*, 1987]. Such extreme horizontal variability of diapycnal mixing rates not only identifies topographic effects as a major cause of heat and salt loss from the Atlantic layer below ice cover, but also predicts the generation of cross-slope density gradients that are presumably geostrophically balanced by alongslope baroclinic currents. Such currents might contribute to the advection of heat and salt around the boundaries of the eastern Arctic Ocean.

As an additional possible effect of the diurnal tide's interaction with topography, we consider briefly the model of tidal rectification proposed by *Loder* [1980]. In this model,

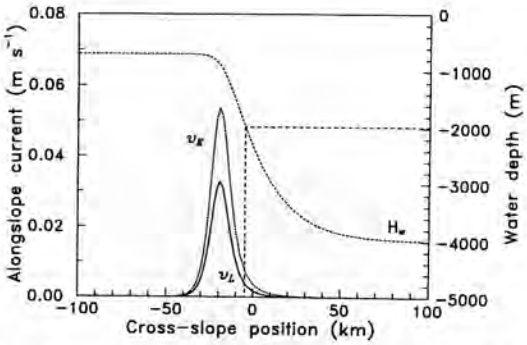

Fig. 14. Along-slope rectified mean Eulerian (v_E) and Lagrangian (v_L) velocity, for idealized Saint-Guily topography representing the northwest slope of the Yermak Plateau, following *Loder* [1980]. Currents are for a deepwater cross-slope flow of 0.04 m s^{-1}, corresponding to predicted spring tides (O_1 and K_1 in phase). The dashed line at 2000 m indicates the approximate position of the O camp over the slope.

the combination of bottom friction and planetary vorticity as a tidal current flows across a topographic slope creates both Eulerian and Lagrangian mean circulations, with the shallow water to the right of the current (in the northern hemisphere). The equations summarizing the strength of this flow are [from *Loder*, 1980, equations 29 and 30]

$$\overline{v_E} \approx -\frac{H_d u_d^2 f \, dH/dx}{2\omega^2 H^2}\left(3\frac{H_d}{H} - 2\right) \tag{6a}$$

$$\overline{v_L} \approx -\frac{H_d u_d^2 f \, dH/dx}{2\omega^2 H^2}\left(2\frac{H_d}{H} - 2\right) \tag{6b}$$

where $\overline{v_E}$ and $\overline{v_L}$ are the Eulerian and Lagrangian alongslope mean velocities, respectively, u_d is the deep water cross-slope velocity, $H(x)$ is the local water depth, and ω is the tidal wave frequency.

Figure 14 shows $\overline{v_E}$ and $\overline{v_L}$ associated with a deep water cross-slope tidal current amplitude of about 0.04 m s^{-1}, chosen to represent spring diurnal tides. The maximum Eulerian current is quite high, about 0.05 m s^{-1}, at the top of the slope, but decreases rapidly inshore of the slope break and toward deeper water. The rectified Lagrangian flow is about 0.01 m s^{-1} toward the northeast, over the midslope ($H_w \approx 2000$ m) sampled during the O camp. This is comparable with the measured mean northeastward flow below the surface stress-driven layer at the O camp cited by *Muench et al.* [1992]. This current was only observed during April 12–22 (days 102–112), but this coincides with the period of maximum cross-slope diurnal currents (Figure 4*a* and 4*d*). If the mechanism is valid in this region, a filament of warm Atlantic Water would be advected into the Arctic Basin clockwise around the perimeter of the plateau by tidal rectification. Such a filament was found in the regional CTD survey during CEAREX [*Muench et al.*, 1992] and might be the "central branch" of the West Spitsbergen Current described by *Lewis and Perkin* [1983] and *Perkin and Lewis* [1984]. Furthermore, the spring-neap modulation of the tidal currents would be echoed in modulation of the rectified flow through the sensitivity of (6) to u_d^2. We are unable at the present time to offer further support for this hypothesis, but it would appear to be a potentially important process in this region.

7. CONCLUSIONS

An analysis of current data from recent experiments near the Yermak Plateau in the eastern Arctic Ocean has confirmed previous observations of locally large diurnal tidal currents in this region. These data have improved the description of the region's diurnal tidal currents, including partial separation of temporal and spatial variability. The principal results of this study are given below.

1. Diurnal currents of up to 0.25 m s^{-1} are found around the perimeter of the northern section of the plateau. The current amplitude and phase are almost constant with depth. Currents over the shallow central plateau and in the deep water surrounding the plateau are smaller than over the upper slope. The major axes of current ellipses are oriented cross-slope. The current ellipses are almost rectilinear at midslope and roughly circular in deeper or shallower water.

2. The cross-slope and vertical structure of the diurnal currents is consistent with a simple model of barotropic, diurnal shelf waves. Such waves are unable to propagate freely around the entire plateau perimeter, invalidating the assumptions of earlier axisymmetric models. We propose that the waves are generated on the eastern side of the plateau, at points where the group velocity is near zero. If this is true, the diurnal variability on the eastern and northwestern flanks of the plateau is due to the large-wavenumber mode of the diurnal shelf wave, in which energy propagates anticlockwise around the plateau while phase propagates clockwise. This forced solution does not depend on a resonance related to the path length of a wave that completely encircles the plateau.

3. Diurnal band spring-neap variability due to temporal beating of the principal diurnal constituents, O_1 and K_1, is a significant component of the observed total modulation. Barotropic shelf waves at these two frequencies have quite different dispersion properties, and the relative efficiency of wave generation and the speeds of energy propagation for each tidal constituent can be very sensitive to local cross-slope bathymetry.

4. The diurnal tide is at least indirectly responsible for the amplification of diapycnal mixing rates [*Padman and Dillon*, 1991] over the plateau slope, as well as acting as a "heat pump" through the surface mixed layer (M. McPhee, personal communication, 1991). Such mixing leads to substantial losses of heat from the Atlantic layer and could generate cross-slope density gradients that would then be geostrophically balanced by along-slope baroclinic currents.

5. The generation of a rectified alongslope flow by the combination of cross-slope tidal currents, planetary vorticity and bottom friction may explain the central branch of the West Spitsbergen Current, a thin filament of warm Atlantic Water advected clockwise around the plateau slope.

6. Under typical conditions, the stress divergence associated with the observed tidal currents is an order of magnitude greater than the divergence of the wind stress. Tidal currents might therefore play a significant role in deformation of the sea ice cover.

While the present study has improved our understanding of the diurnal tide near the Yermak Plateau, there are several aspects that remain speculative. There is now, however, ample evidence that the interaction of the diurnal tidal currents with topography plays a significant role in establishing the regional hydrographic and circulation properties.

The spatial variability of tidal currents must therefore be taken into account in basin-scale circulation models of the Arctic Ocean. Further effort, such as improving the resolution of the *Gjevik* [1990] numerical tidal model, is therefore justified in terms of improved modeling of larger-scale oceanographic processes. A better bathymetric data base is also required, given the shelf waves' sensitivity to cross-slope topographic scales.

Acknowledgments. We are pleased to acknowledge the assistance provided by the following people. Bjørn Gjevik provided considerable advice on tidal models of the eastern Arctic Ocean. Dave Chapman is thanked for discussions on slope-trapped waves. Miles McPhee provided the navigation data for the *Polarbjørn* and *Polarqueen* ship drifts, and Knut Aagaard provided current meter tidal band spectral levels and tidal coefficients. This work was supported by the Office of Naval Research, contracts N00014-87-K-0009 and N00014-90-J-1042 (L.P.), N00014-84-C-0134 (A.J.P.), N00014-82-C-0064 and N00014-91-C-0030 (R.D.M.), and N00014-90-J-1099 (R.P.). WHOI contribution 7732.

REFERENCES

Aagaard, K., A synthesis of Arctic Ocean circulation, *Rapp. P. V. Reun. Cons. Int. Explor. Mer, 188*, 11–22, 1989.

Aagaard, K., A. Foldvik, T. Gammelsrød, and T. Vine, One-year records of current and bottom pressure in the strait between Nordaustlandet and Kvitøya, Svalbard, 1980–81, *Polar Res., 1*, 107–113, 1983.

Brink, K. H., and D. C. Chapman, Programs for computing properties of coastal-trapped waves and wind-driven motions over the continental shelf and slope (2nd ed.), *Tech. Rep. WHOI-87-24*, Woods Hole Oceanogr. Inst., Woods Hole, Mass., 1987.

Chapman, D. C., Enhanced subinertial diurnal tides over isolated topographic features, *Deep Sea Res., 36*, 815–824, 1989.

Chapman, D. C., and M. C. Hendershott, Shelf wave dispersion in a geophysical ocean, *Dyn. Atmos. Oceans, 7*, 17–31, 1982.

Czipott, P. V., M. D. Levine, C. A. Paulson, D. Menemenlis, D. M. Farmer, and R. G. Williams, Ice flexure forced by internal wave packets in the Arctic Ocean, *Science, 254*, 832–835, 1991.

D'Asaro, E. A., and J. H. Morison, Internal waves and mixing in the Arctic Ocean, *Deep Sea Res.*, in press, 1992.

Gjevik, B., Model simulations of tides and shelf waves along the shelves of the Norwegian-Greenland-Barents Sea, in *Modeling Marine Systems*, vol. 1, edited by A. M. Davies, pp. 187–219, CRC Press, Boca Raton, Fla., 1990.

Gjevik, B., and T. Straume, Model simulations of the M_2 and K_1 tide in the Nordic seas and the Arctic Ocean, *Tellus, 41*, 73–96, 1989.

Gregg, M. C., Diapycnal mixing in the thermocline: A review, *J. Geophys. Res., 92*, 5249–5286, 1987.

Gregg, M. C., Scaling turbulent dissipation in the thermocline, *J. Geophys. Res., 94*, 9686–9698, 1989.

Hoffman, P. J., Transpolar sea ice drift in the vicinity of the Yermak Plateau as observed by Arctemiz 86 buoys, M.S. thesis, 99 pp., Nav. Postgrad. Sch., Monterey, Calif., 1990.

Honjo, S., R. Krishfield, and A. J. Plueddemann, The Arctic environmental drifting buoy (AEDB): Report of field operations and results, *Tech. Rep. WHOI 90-02*, 128 pp., Woods Hole Oceanogr. Inst., Woods Hole, Mass., 1990.

Hunkins, K., Current and temperature data from instrument moorings in Fram Strait during MIZEX 83, *Tech. Rep. LDGO-84-1*, 69 pp., Lamont-Doherty Geol. Observ., Palisades, N.Y., 1984.

Hunkins, K., Anomalous diurnal tidal currents on the Yermak Plateau, *J. Mar. Res., 44*, 51–69, 1986.

Huthnance, J. M., Large tidal currents near Bear Island and related tidal energy losses from the North Atlantic, *Deep Sea Res., 28*, 51–70, 1981.

Jackson, H. R., G. L. Johnson, E. Sundoor, and A. M. Myhre, The Yermak Plateau: Formed at a triple junction, *J. Geophys. Res., 89*, 3223–3232, 1984.

Johannessen, O., Note on some vertical profiles below ice floes in the Gulf of St. Lawrence and near the North Pole, *J. Geophys. Res., 75*, 2857–2862, 1970.

Johnson, G. L., The FRAM Expeditions: Arctic Ocean studies from floating sea ice, 1979–1982, *Polar Rec., 21*, 583–589, 1983.

Langleben, M. P., Water drag coefficient at AIDJEX, Station Caribou, in *Sea Ice Processes and Models*, edited by R. S. Pritchard, pp. 464–471, University of Washington Press, Seattle, 1980.

Lewis, E. L., and R. G. Perkin, Supercooling and energy exchange near the Arctic Ocean surface, *J. Geophys. Res., 88*, 7681–7685, 1983.

Loder, J. W., Topographic rectification of tidal currents on the sides of Georges Bank, *J. Phys. Oceanogr., 10*, 1399–1416, 1980.

McPhee, M. G., Drift velocity during the drift-station phase of MIZEX 83, *MIZEX Bull. IV, CRREL Spec. Rep. 84-28*, U.S. Army Cold Reg. Res. and Eng. Lab., Hanover, N. H., 1984.

McPhee, M. G., Analysis and prediction of short-term ice drift, *J. Offshore Mech. Arct. Eng., 110*, 94–100, 1988.

Middleton, J. H., T. D. Foster, and A. Foldvik, Diurnal shelf waves in the southern Weddell Sea, *J. Phys. Oceanogr., 17*, 784–791, 1987.

Morison, J. H., M. G. McPhee, and G. A. Maykut, Boundary layer, upper ocean, and ice observations in the Greenland Sea marginal ice zone, *J. Geophys. Res., 92*, 6987–7011, 1987.

Moritz, R. E., and R. Colony, Statistics of sea ice motion, Fram Strait to the North Pole, *Proc.* (4), *Int. Conf. Offshore Mech. Arct. Eng., 7th*, 75–82, 1987.

Muench, R. D., G. S. E. Lagerloef, and J. T. Gunn, 1984–85 current observations in the East Greenland Current: A preliminary description, *MIZEX Bull. VII*, U.S. Army Cold Reg. Res. and Eng. Lab., Hanover, N. H., 1986.

Muench, R. D., M. G. McPhee, C. A. Paulson, and J. H. Morison, Winter oceanographic conditions in the Fram Strait–Yermak Plateau region, *J. Geophys. Res., 97*, 3469–3483, 1992.

Padman, L., and T. M. Dillon, Vertical heat fluxes through the Beaufort Sea thermohaline staircase, *J. Geophys. Res., 92*, 10,799–10,806, 1987.

Padman, L., and T. M. Dillon, Turbulent mixing near the Yermak Plateau during the Coordinated Eastern Arctic Experiment, *J. Geophys. Res., 96*, 4769–4782, 1991.

Padman, L., T. M. Dillon, H. W. Wijesekera, M. D. Levine, C. A. Paulson, and R. Pinkel, Internal wave mixing in a non-Garrett-Munk ocean, in *Proceedings of the 'Aha Huliko'a Hawaiian Winter Workshop*, pp. 31–51, University of Hawaii at Manoa, Honolulu, 1991.

Perkin, R. G., and E. L. Lewis, Mixing in the West Spitsbergen Current, *J. Phys. Oceanogr., 14*, 1315–1325, 1984.

Pinkel, R., and J. A. Smith, Repeat-sequence coding for improved precision of Doppler sonar, *J. Atmos. Oceanic Technol., 9*, 149–163, 1992.

Plueddemann, A. J., Internal wave observations from the Arctic environmental drifting buoy, *J. Geophys. Res.*, this issue.

Prazuck, C., Anomalous diurnal currents in the vicinity of the Yermak Plateau, Ph.D. dissertation, 125 pp., Nav. Postgrad. Sch., Monterey, Calif., 1991.

Saint-Guily, B., Sur la propagation des ondes de seconde classe le long d'un talus continental, *C. R. Acad. Sci. Paris, Ser. B, 282*, 141–144, 1976.

Schwiderski, E. W., On charting global ocean tides, *Rev. Geophys., 18*, 243–268, 1980.

Thomson, R. E., and W. A. Crawford, The generation of diurnal period shelf waves by tidal currents, *J. Phys. Oceanogr., 12*, 635–643, 1982.

R. D. Muench, Science Applications International Corporation, 13400B Northrup Way, Suite 36, Bellevue, WA 98005.

L. Padman, College of Oceanography, Oregon State University, Corvallis, OR 97331.

R. Pinkel, Marine Physical Laboratory, Scripps Institution of Oceanography, La Jolla, CA 92093.

A. J. Plueddemann, Department of Physical Oceanography, Woods Hole Oceanographic Institution, Woods Hole, MA 02543.

(Received November 13, 1991;
accepted March 23, 1992.)